electronics

MDPI

Article

Design and Fabrication of a Compact Branch-Line Coupler Using Resonators with Wide Harmonics Suppression Band

Sobhan Roshani [1], Salah I. Yahya [2,3], Saeed Roshani [1,*] and Meysam Rostami [1]

1 Department of Electrical Engineering, Kermanshah Branch, Islamic Azad University, Kermanshah 6718997551, Iran; sobhan_roshany@yahoo.ca (S.R.); meysamrostami@yahoo.com (M.R.)
2 Department of Communication and Computer Engineering, Cihan University-Erbil, Erbil 44001, Iraq; salah.ismaeel@koyauniversity.org
3 Department of Software Engineering, Faculty of Engineering, Koya University, Koya KOY45, Iraq
* Correspondence: s_roshany@yahoo.com

Abstract: The branch-line coupler (BLC) is an important device in radio frequency (RF) and microwave (MW) circuits. The main drawbacks of the conventional BLC are as follows: first, the four long quarter-wavelength (λ/4) transmission line sections occupy a large size, especially at the low frequencies, and second, the presence of unwanted harmonics. This research paper presents a compact 750 MHz BLC with harmonics suppression using resonators. The typical BLC consists of four λ/4 branches, two series arms of 35 Ω and two shunt arms of 50 Ω impedances. In the proposed BLC, these long branches are replaced with two types of compact resonators. The proposed resonators have the same responses at the operating frequency of 750 MHz and suppress higher frequencies. The designed BLC is simulated, fabricated and measured. The results show that the proposed BLC has good performance at 750 MHz with a bandwidth of 200 MHz, which provides more than 26% fractional bandwidth (FBW). It has a very compact size, about 84% size reduction, as compared with the typical BLC. Moreover, the fabricated BLC suppresses the 2nd up to 7th unwanted harmonics with a high suppression level.

Keywords: low-pass filter (LPF); elliptical resonator; stopband; passband; 5G

Citation: Roshani, S.; Yahya, S.I.; Roshani, S.; Rostami, M. Design and Fabrication of a Compact Branch-Line Coupler Using Resonators with Wide Harmonics Suppression Band. *Electronics* **2022**, *11*, 793. https://doi.org/10.3390/electronics11050793

Academic Editor: Raed A. Abd-Alhameed

Received: 29 January 2022
Accepted: 2 March 2022
Published: 3 March 2022

1. Introduction

Couplers are widely used in radio frequency (RF) and microwave (MW) circuits for combining/dividing input power [1]. The typical branch-line coupler (BLC) consists of four λ/4 branches. It consists of two series arms with 35 Ω and two shunt arms with 50 Ω impedances, which make this component undesirably large, especially at low frequencies, and susceptible to unwanted harmonics. The typical BLC passes all unwanted harmonics along with the main signal.

So far, various techniques have been reported to miniaturize the branch-line coupler structure and/or suppress the harmonics.

In many designs [2–5], low-pass filters (LPFs) are used as the coupler branches to miniaturize the structure and suppress the harmonics. This technique gives good results but increases the design complexity and the insertion loss.

Other techniques [6–9] have used external lumped components, such as capacitors and inductors, to overcome the structure's large size and the presence of harmonics in typical BLCs. Applying lumped reactive components significantly reduces the circuit size and rejects unwanted harmonics but limits the frequency range.

Several works [10–16] have used a defected ground structure (DGS), photonic bandgap (PBG) cells and electromagnetic bandgap (EBG) cells for cancelling the harmonics and reducing the large size of BLCs. These cells need an extra implementation process, which increases the design complexity. Moreover, recently, the crystal photonic structures were used for higher-frequency circuits, which can be used for coupler structures [17–25].

Applying open-ended stubs is another effective method, which was previously widely used to modify typical couplers [26–31]. Using open stubs in couplers leads to achieving a simple structure. However, in this method, each open stub produces only a single transmission zero, which cannot provide a wide rejection band.

The coupled line structure [32–35] is another method that provides a bandpass response and impressively rejects other frequencies. Because of the coupled structure, the insertion loss is very high in this method.

In the design process of the coupler, to achieve the best performance, the dimensions of the applied stubs should be tuned. In [36–39], compact couplers are investigated for which the size reductions are not significant. To find the optimal dimensions of applied stubs and also to solve a variety of engineering problems, several models, artificial intelligence methods [40–49], and neural networks are used [50–66]. Additionally, artificial intelligence methods have been utilized to design microwave devices, such as power dividers and couplers [67,68].

In this work, two types of resonators are applied instead of the two types of long branches in the typical BLC. The applied method efficiently reduces the size of the circuit and eliminates undesirable harmonics.

2. The Conventional Coupler

The typical BLC consists of four λ/4 branches, two series arms of 35 Ω and two shunt arms of 50 Ω impedances. The schematic diagram of the conventional BLC is depicted in Figure 1a. The microstrip realization of the conventional BLC with RT/Duroid-5880 substrate of 5 mil thickness, ε_r = 2.2 and loss tan = 0.0009 at 750 MHz is shown in Figure 1b. The conventional BLC has a large size of 73 mm × 73 mm (0.25 λ × 0.25 λ) and passes higher frequencies along with the signal without any suppression. The EM frequency response of the typical BLC is depicted in Figure 1c.

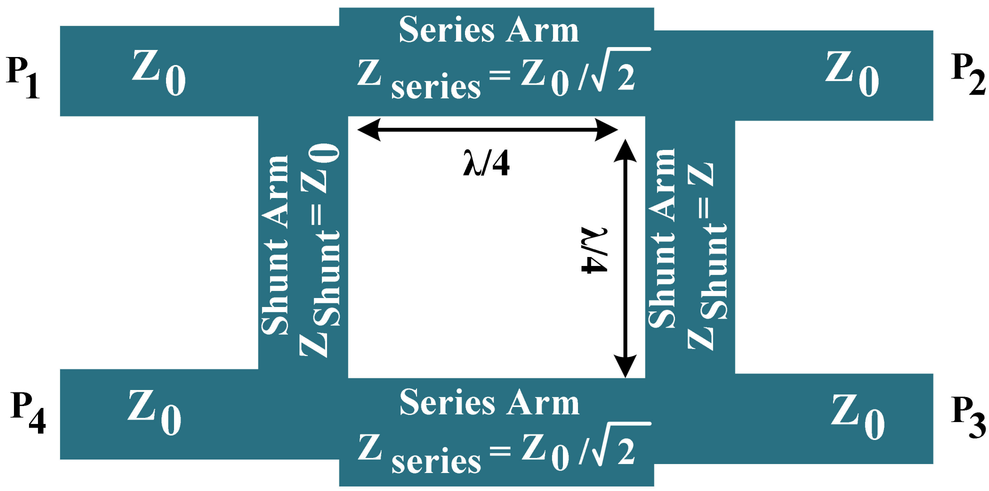

(**a**)

Figure 1. *Cont.*

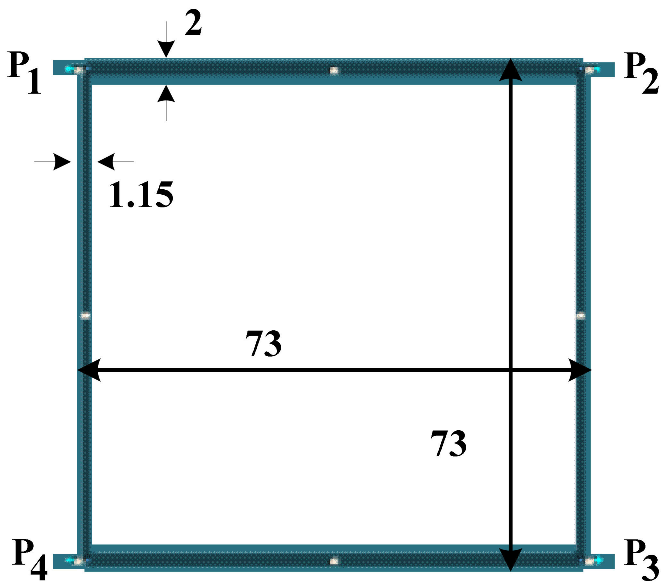

(**b**)

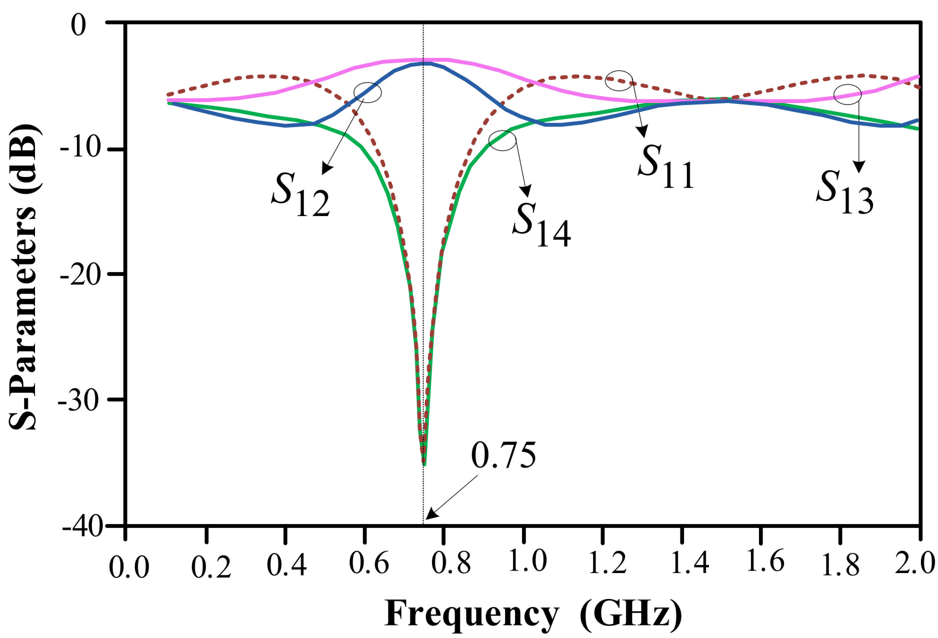

(**c**)

Figure 1. Conventional 750 MHz BLC: (**a**) schematic diagram, (**b**) layout, and (**c**) frequency response. Dimensions are in millimeters.

3. Proposed Resonators

The BLC consists of two horizontal series lines of 35 Ω and two vertical shunt lines of 50 Ω impedances. In the proposed structure, two vertical resonators are used instead of the two long vertical branches, and two horizontal resonators are used instead of the two long horizontal branches.

3.1. Design Procedure of the Proposed Circuit

The design procedure of the proposed coupler is graphically explained in Figure 2. The conventional BLC at 750 MHz is designed at Step 1, which has a large size and suffers from the presence of unwanted harmonics in its frequency response. The conventional BLC consists of two long series branches and two long shunt branches. In Step 2, at first, the LC model resonator is presented, and related equations are extracted. Then, the TZ location can be obtained by equating the input impedance to zero. In addition, the TZ location can be adjusted by tuning the lumped element values in the LC circuit. In Step 3, two compact resonators are realized based on the proposed LC model, which are used instead of the long branches of the conventional coupler. The obtained resonators are used to form preliminary prototype of the coupler in Step 4, and the final coupler structure is achieved in Step 5 by adding four extra resonators.

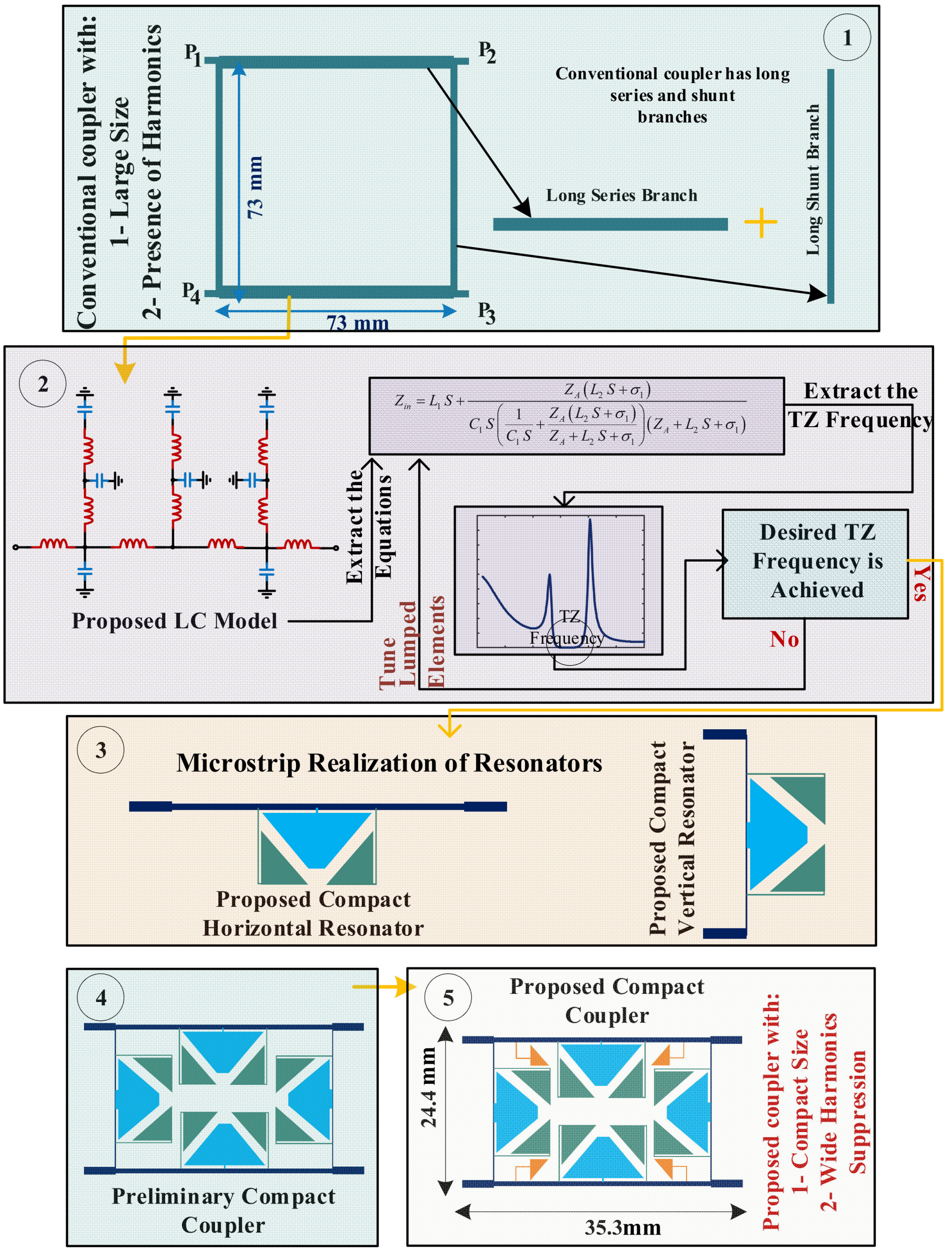

Figure 2. Design procedure of the proposed coupler. In this figure, the design steps of the proposed circuit are explained in 5 steps.

3.2. Vertical Branches

The structure of the vertical λ/4 branch with 50 Ω (w = 1.15 mm) is depicted in Figure 3a. The frequency response of this vertical line is depicted in Figure 3b. As the results show, the vertical λ/4 branch easily passes the signal at 750 MHz without any attenuation (S_{12} near zero), and the S_{11} parameter is more than 10 dB. Note that S_{12} = S_{21}, as the BLC is a reciprocal passive component. Unfortunately, this line passes other higher frequency signals without any attenuation (S_{12} near zero), exactly like the main signal.

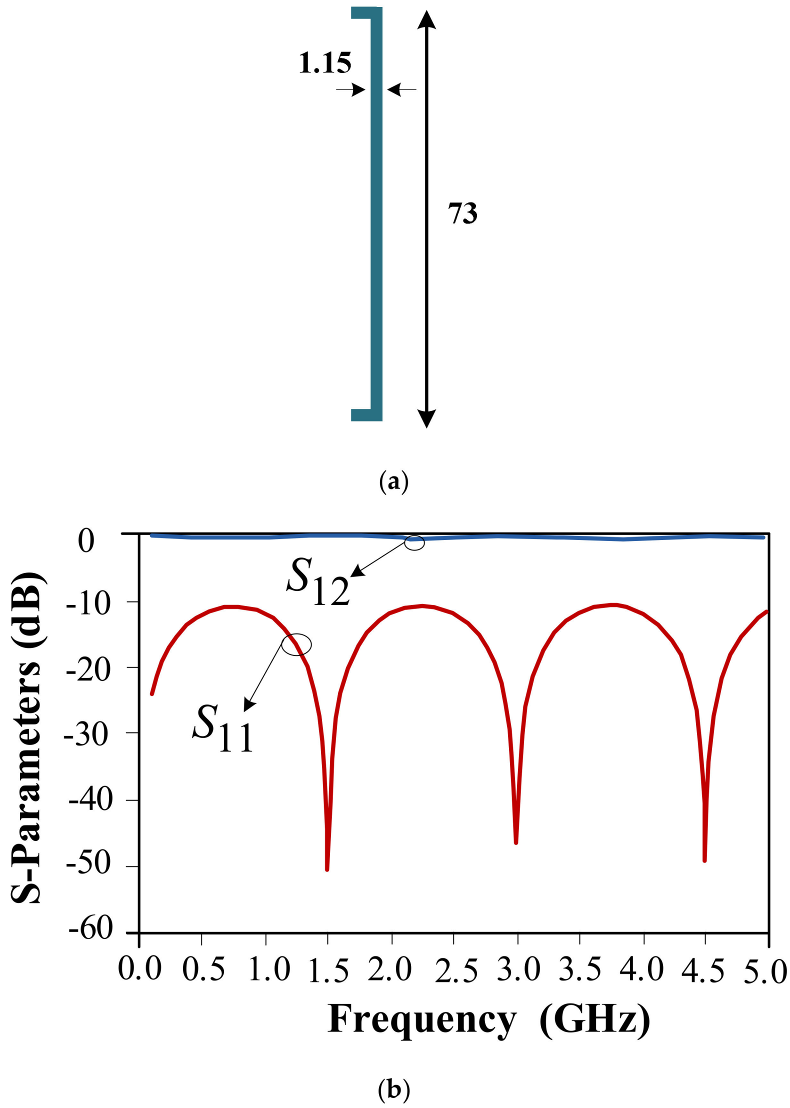

Figure 3. Vertical λ/4 branch of 50 Ω impedance at 750 MHz; (**a**) layout with dimensions in millimeters, and (**b**) the simulation of the S_{11} and S_{12} magnitudes in decibels.

3.3. Horizontal Branches

The structure of the horizontal λ/4 branch with 35 Ω (w = 2 mm) is depicted in Figure 4a. The frequency response of this horizontal line is shown in Figure 4b. As the results show, the horizontal λ/4 branch easily passes the signal at 750 MHz without any attenuation (S_{12} near zero), and the S_{11} parameter is more than 20 dB. Unfortunately, this line passes other signals at higher frequencies without any attenuation (S_{12} near zero), exactly like the main signal.

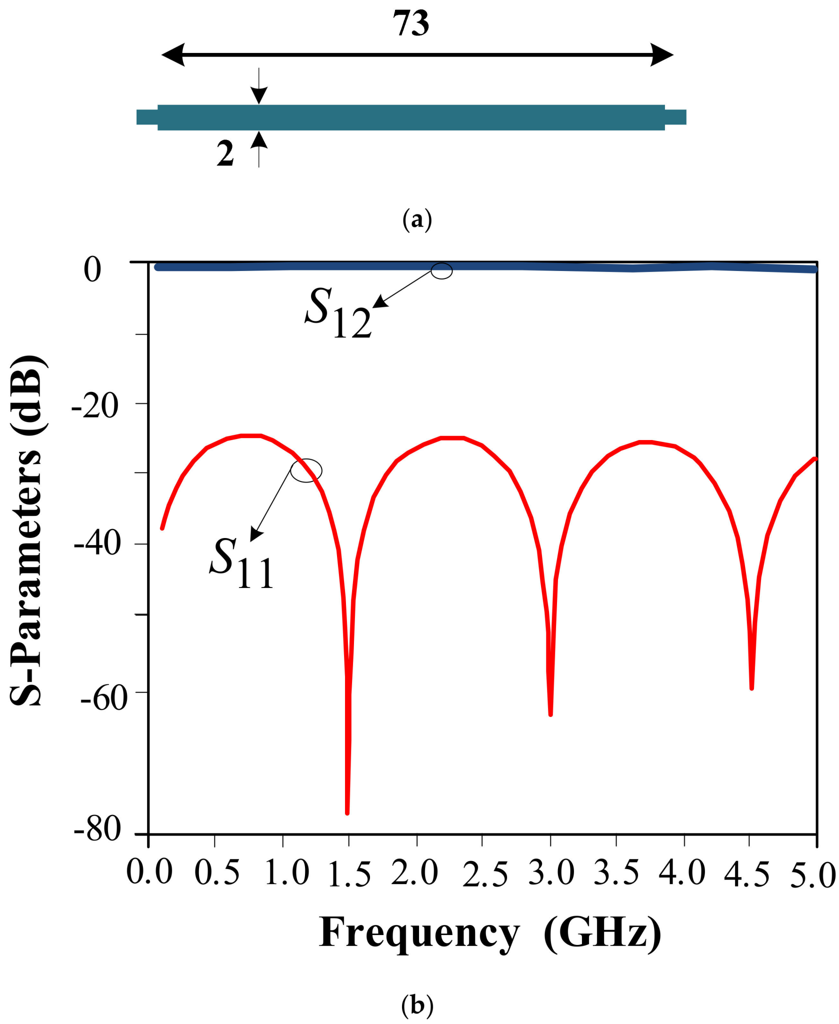

Figure 4. Horizontal λ/4 branch of 35 Ω impedance at 750 MHz; (**a**) layout with dimensions in millimeters and (**b**) the simulation of the S_{11} and S_{12} magnitudes in decibels.

These vertical and horizontal lines have the same length of λ/4, but their widths are different. In the proposed design, triangular shaped resonators are used to improve the performance of the coupler.

3.4. Proposed Vertical Resonator

The layout structure of the proposed vertical resonator is depicted in Figure 5. This resonator consists of a triangle-shaped resonator at the middle and two flag-shaped suppressing cells on both sides.

The dimensions of the applied stubs in the proposed vertical resonator are listed as follows: L_{b1} = 4.1, W_{b1} = 0.6, L_{b2} = 19.6, L_{b3} = 5.6, W_{b2} = 0.1 (all in millimeters). The frequency responses of the proposed vertical resonator are depicted in Figure 6. The designed structure easily passes 750 MHz, like the vertical line, and also creates a strong transmission zero at 1.7 GHz frequency.

The LC-equivalent (LCE) model of the proposed vertical resonator is extracted as illustrated in Figure 7.

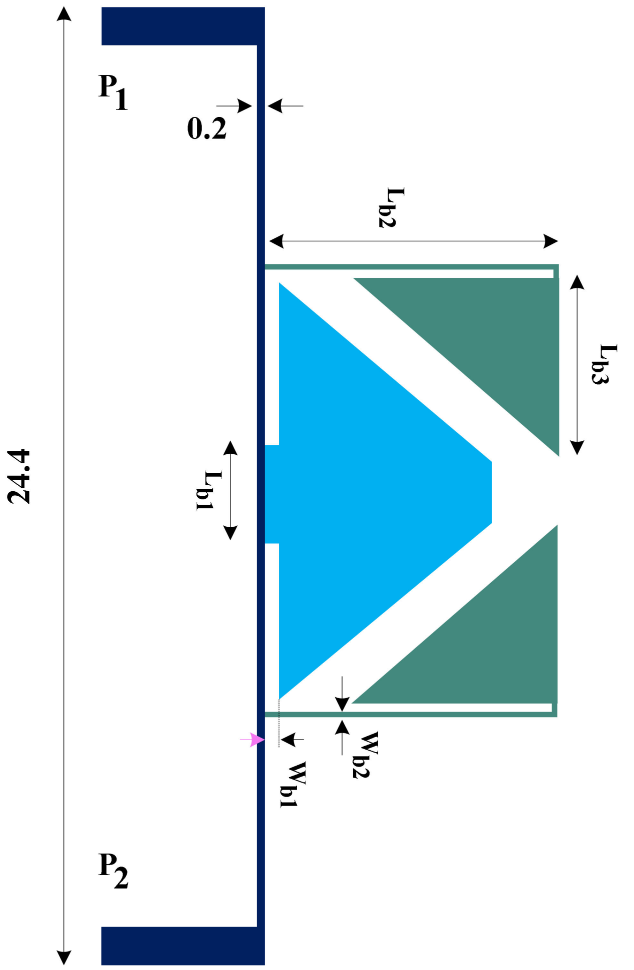

Figure 5. The layout of the proposed vertical resonator.

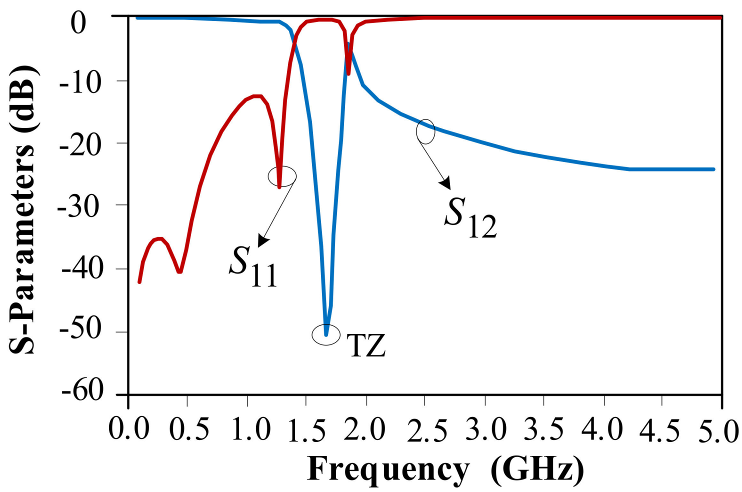

Figure 6. The S_{11} and S_{12} magnitudes in decibels versus frequency.

The extracted LCE model has an asymmetrical structure, where the obtained values for the applied lumped reactive elements are listed in Table 1.

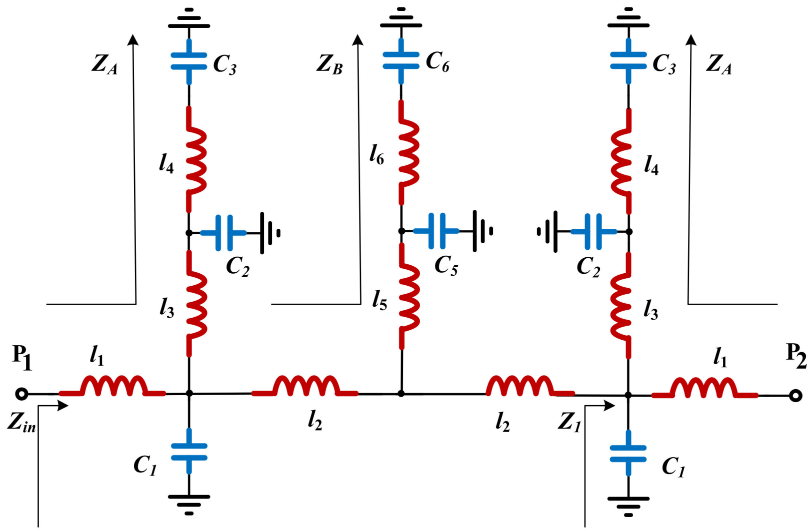

Figure 7. Extracted LCE model of the proposed vertical resonator.

Table 1. Obtained values for the applied lumped elements of the LC model of the resonator.

Parameters	L_1	L_2	L_3	L_4	L_5	L_6
Values (nH)	2.1	2.3	5.2	0.4	0.15	0.15
Parameters	C_1	C_2	C_3	C_4	C_5	C_6
Values (pF)	1	1	0.87	6	1.2	1.2

In Figure 8, the EM simulation of the proposed vertical resonator and its LCE model simulation response are compared. In this figure, the LCE model is simulated with a circuit simulator and the vertical resonator is simulated with electromagnetic (EM) simulation in Advanced Design System (ADS) software. There is good agreement between these responses, which shows the validity of the LCE model.

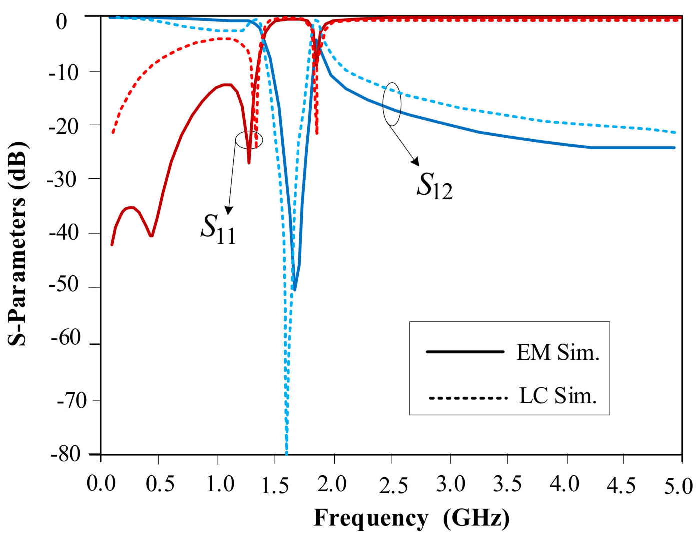

Figure 8. EM simulation of the proposed vertical resonator and its LCE model response.

The values of Z_A, and Z_B (which are indicated in Figure 7) can be calculated according to the following equations:

$$Z_A = L_3\,S + \frac{\frac{1}{C_3\,S} + L_4\,S}{C_2\,S\left(\frac{1}{C_2\,S} + \frac{1}{C_3\,S} + L_4\,S\right)} \tag{1}$$

$$Z_B = L_5\,S + \frac{\frac{1}{C_6\,S} + L_6\,S}{C_5\,S\left(\frac{1}{C_5\,S} + \frac{1}{C_6\,S} + L_6\,S\right)} \tag{2}$$

where, "S" refers to the Laplace transform. The input impedances, indicated in Figure 7 by Z_1 and Z_{in}, can be extracted based on Equations (1) and (2), which are written in Equations (3)–(5).

$$Z_1 = \frac{Z_A\,(R + L_1\,S)}{C_1\,S\left(Z_A + \frac{R+L_1\,S}{C_1\,S\left(R+\frac{1}{C_1\,S}+L_1\,S\right)}\right)\left(R + \frac{1}{C_1\,S} + L_1\,S\right)} \tag{3}$$

$$Z_{in} = L_1\,S + \frac{Z_A\,(L_2\,S + \sigma_1)}{C_1\,S\left(\frac{1}{C_1\,S} + \frac{Z_A\,(L_2\,S+\sigma_1)}{Z_A+L_2\,S+\sigma_1}\right)(Z_A + L_2\,S + \sigma_1)} \tag{4}$$

$$\sigma_1 = \frac{Z_B\,(L_2\,S + Z_1)}{Z_B + L_2\,S + Z_1} \tag{5}$$

where "R" refers to 50 Ω impedance at port 2, and "σ_1" is a parameter defined in Equation (5) to simplify the Z_{in} equation. The real part of the input impedance Z_{in} is shown in Figure 9. The TZ location can be obtained by equating the input impedance to zero. Additionally, the TZ location can be adjusted by tuning the lumped element values in the LC circuit.

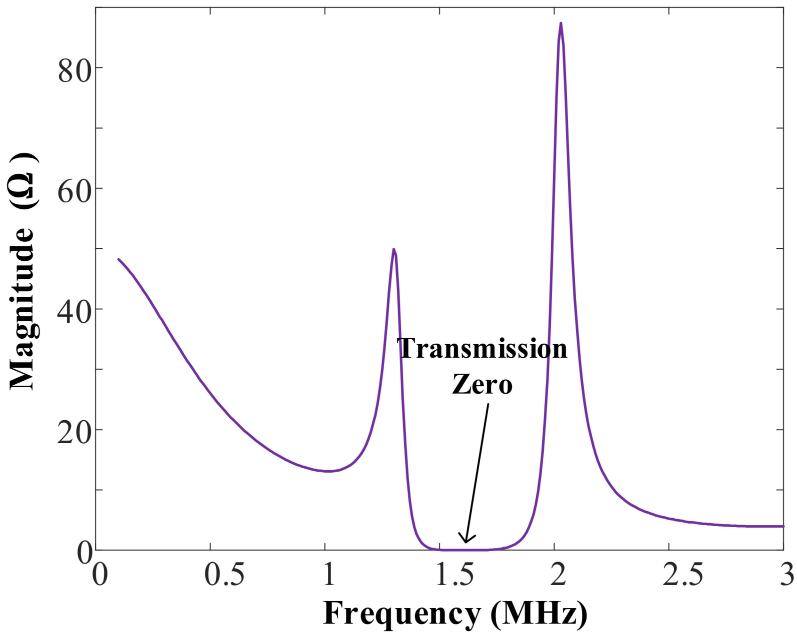

Figure 9. The real part of the input impedance Z_{in}.

3.5. Proposed Horizontal Resonator

The horizontal resonator is used instead of the 35 Ω series arm, and this is very similar to the vertical resonator because the horizontal arm and series arm have the same structure, same length and only a little difference in the line thickness. The layout structure of the horizontal resonator is depicted in Figure 10.

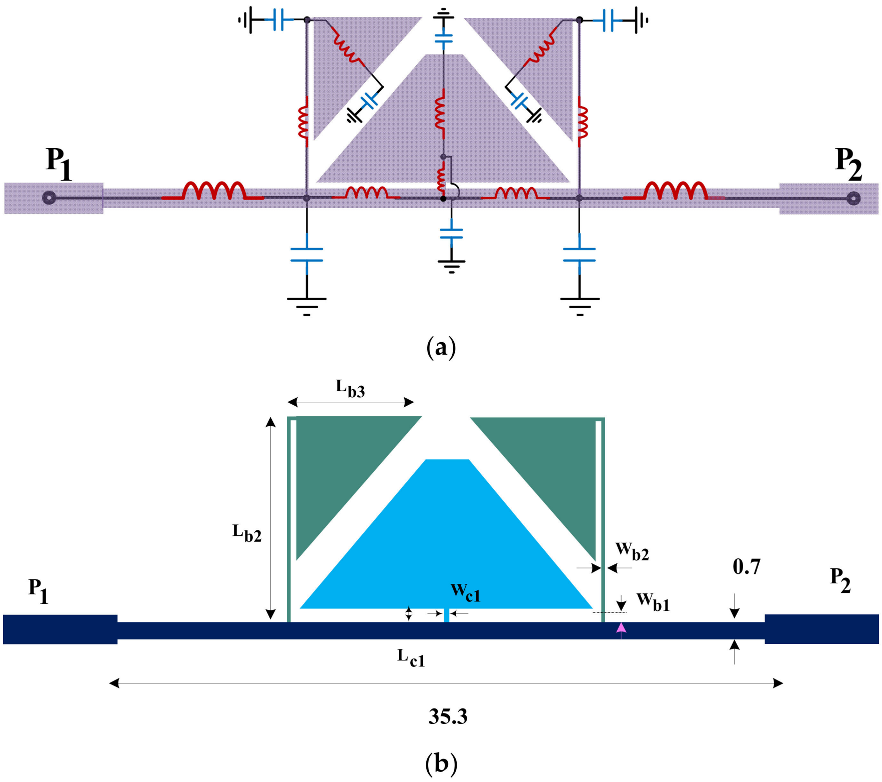

Figure 10. Layout of the proposed horizontal resonator. (**a**) Layout extraction of the resonator from the LC equivalent circuit. (**b**) Dimensions of the proposed horizontal resonator.

The dimensions of the applied stubs in the proposed horizontal resonator are listed as follows: Lc1 = 0.7, Lb2 = 19.6, Lb3 = 5.6, Wc1 = 0.1, Wb1 = 0.6, Wb2 = 0.1 (all in millimeters). The EM simulation response of the proposed horizontal resonator is illustrated in Figure 11. The proposed structure easily passes 750 MHz, like the simple horizontal line, and also creates a strong transmission zero at 1.6 GHz frequency.

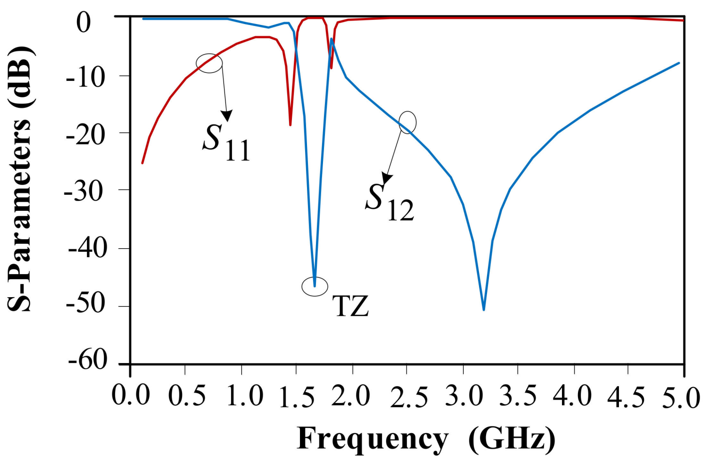

Figure 11. EM simulation response of the proposed horizontal resonator.

3.6. The LC Models of the Preliminary and the Final Prototypes of the Coupler

The LCE model for the preliminary and the final prototypes of the coupler are depicted in Figure 12a. In the LCE circuit, C_Z and L_Z only exist in the final prototypes of the coupler, i.e., by adding four series LC branches containing C_Z and L_Z in the preliminary prototype, the final prototype of the coupler is constructed. The horizontal LC values in the LCE circuit of the final prototype of the coupler are the same as the values in Table 1. However, according to the impedance difference in the vertical branches of the coupler, the vertical LC values in the LCE circuit of the final prototype of the coupler are tuned, which are listed in Table 2. The comparison between the LCE model frequency responses of the preliminary and the final prototypes of the coupler are shown in Figure 12b, which shows acceptable results with a wide rejection band.

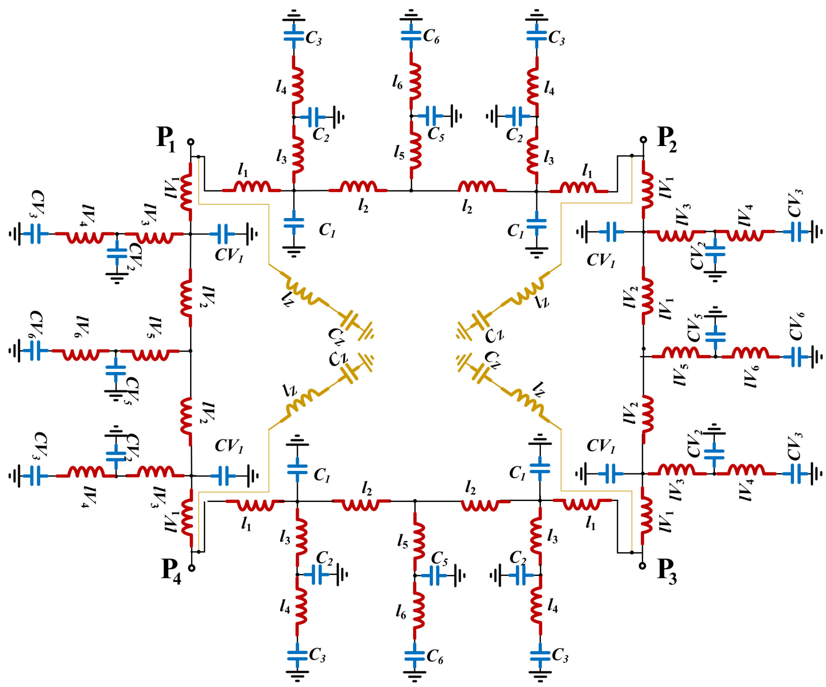

(**a**)

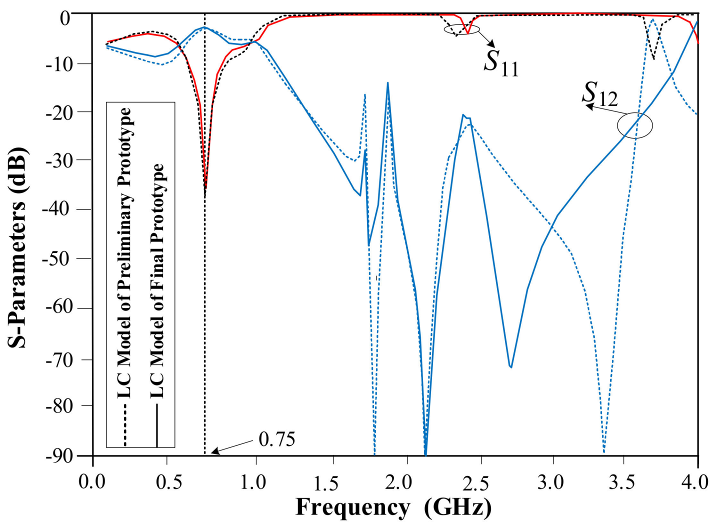

(**b**)

Figure 12. (**a**) The LCE models of the preliminary and the final prototypes of the coupler. (**b**) The comparison between LCE model frequency responses of the preliminary and the final prototypes of the coupler. In LCE circuit, C_Z and L_Z only exist in the final prototypes of the coupler.

Table 2. Obtained values for the applied lumped elements of the LC model of the coupler.

Parameters	LV_1	LV_2	LV_3	LV_4	LV_5	LV_6
Values (nH)	1	6.3	5.2	0.4	0.18	0.18
Parameters	CV_1	CV_2	CV_3	CV_4	CV_5	CV_6
Values (pF)	5.4	1	0.87	6	1.2	1.2

4. Proposed Coupler Design

In the proposed coupler design process, the horizontal and vertical resonators are used instead of four long branches.

4.1. The Preliminary Prototype of the Designed Coupler

The preliminary prototype of the designed coupler is designed by placing vertical and horizontal resonators instead of the vertical and horizontal lines. The structure and frequency responses of the preliminary prototype of the designed coupler are shown in Figure 13. This coupler rejects the third to sixth harmonics and provides wide rejection bands from 1.75 GHz to 3.85 GHz, with more than a 20 dB attenuation level.

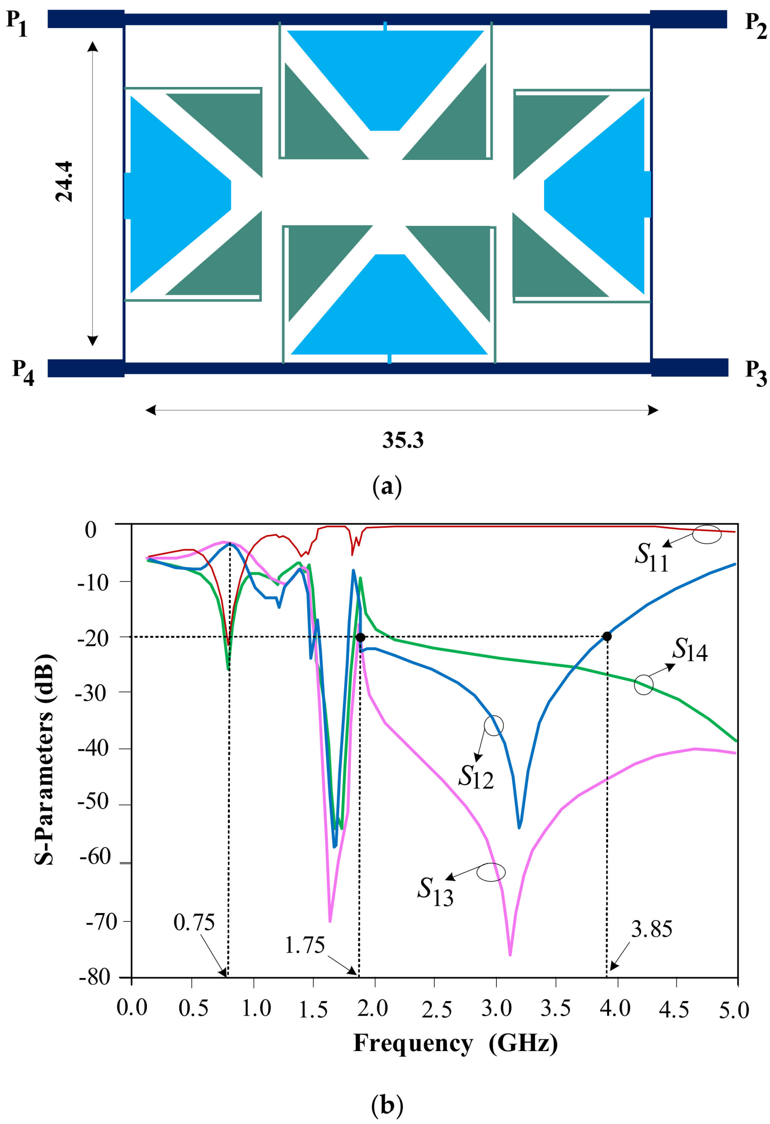

Figure 13. The preliminary prototype of the designed coupler; (**a**) layout with dimensions in millimeters, and (**b**) EM simulation response.

4.2. The Final Prototype of the Designed Coupler

The preliminary prototype of the designed coupler only eliminates the third to sixth harmonics, but it does not have the ability to suppress the second harmonic. To remove the second harmonic, four small triangular shaped open-ended stubs are added in the final prototype of the deigned coupler. The added triangular open-ended stubs can create extra transmission zeros, which helps to improve the harmonic suppression in the device [69,70]. The structure and S-parameters curves of the final prototype of the designed coupler are shown in Figure 14. This coupler rejects the second to seventh harmonics and provides a wide rejection band from 1.5 GHz to 5.4 GHz.

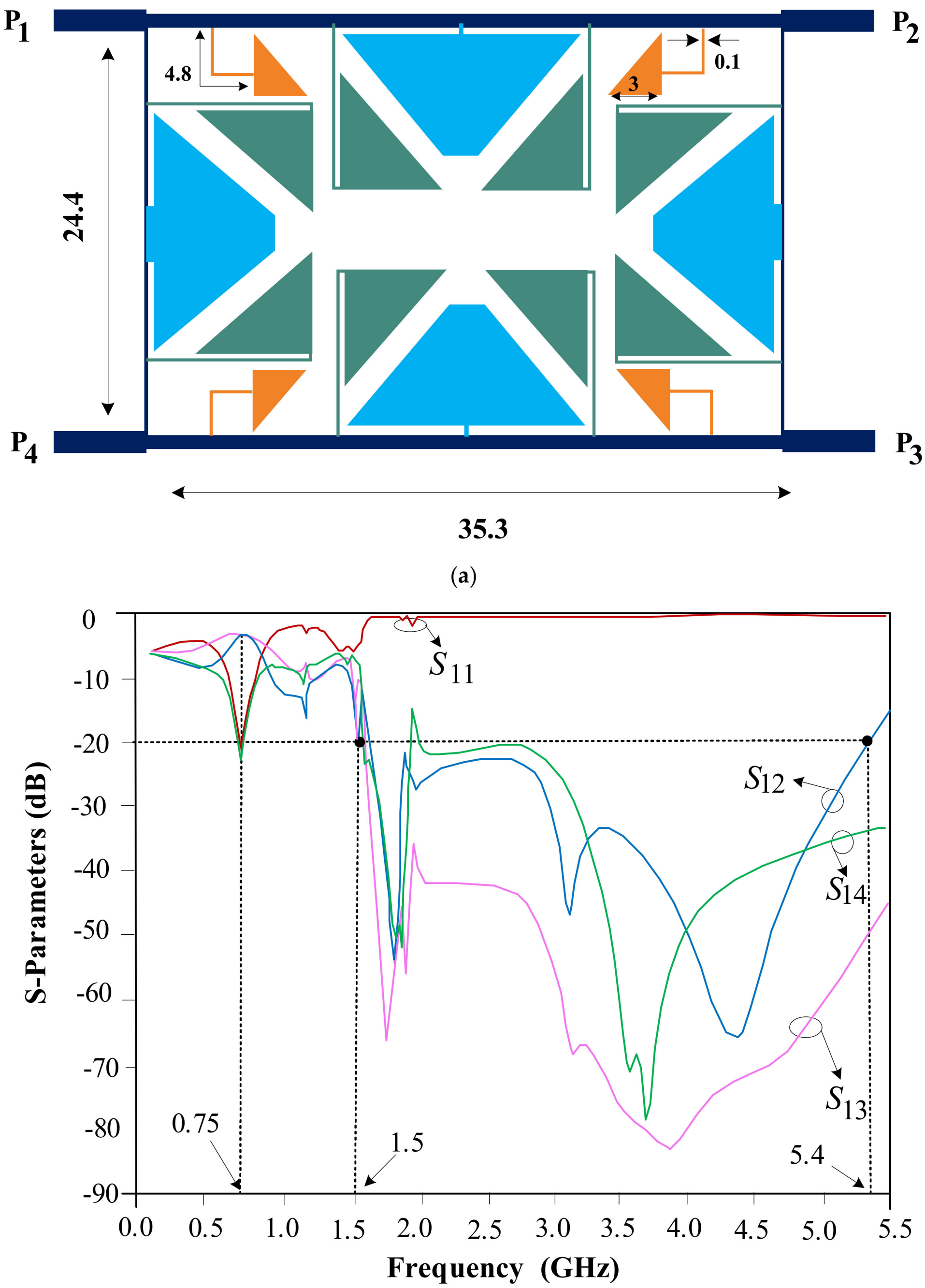

(**b**)

Figure 14. The final prototype of the designed coupler; (**a**) layout with dimensions in millimeters, and (**b**) EM simulation response.

5. Fabrication and Measurements

The final prototype of the designed BLC is fabricated on a substrate of Rogers RT-5880 substrate with 15 mil thickness, εr = 2.2 and loss tan = 0.0009. The photo of the fabricated BLC is presented in Figure 15.

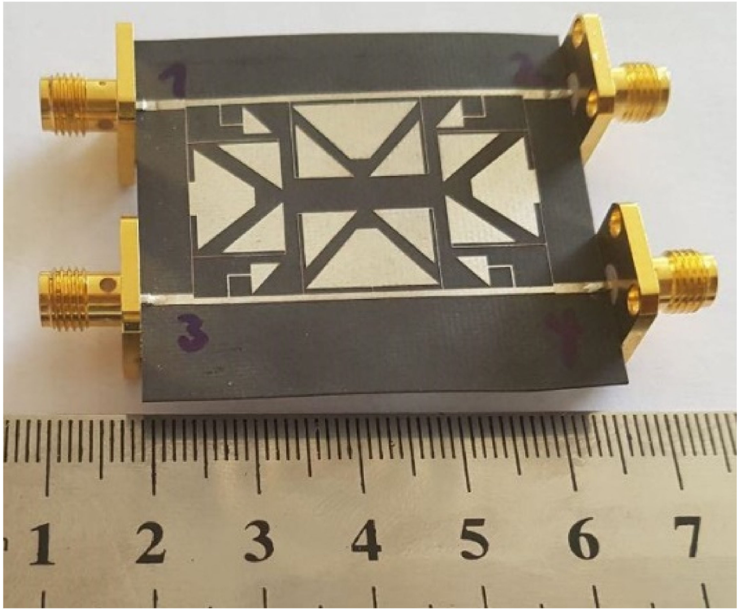

Figure 15. Photograph of the fabricated BLC.

The conventional coupler has a size of 0.25 × 0.25 λg^2, whereas the size of the final prototype of the designed coupler is only 0.08 × 0.12 λg^2 (24.4 × 35.3 mm^2), where λg is obtained at 750 MHz working frequency. The final prototype of the designed BLC demonstrates an 84% size reduction, in comparison with the typical BLC. The layout of the proposed and conventional couplers, which is designed on the same substitute and operates at the same frequency, is depicted in Figure 16, which shows an extreme size reduction in the final prototype of the designed coupler.

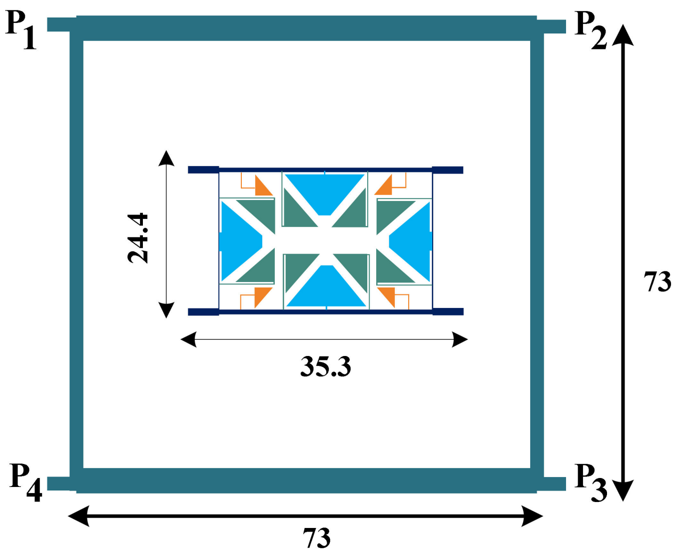

Figure 16. Layouts comparison between the final prototype of the designed coupler (24.4 mm × 35.3 mm) and the conventional couplers (73 mm × 73 mm) at 750 MHz.

The simulated and measured S-parameters of the final prototype of the designed BLC are depicted in Figure 17. As seen from the obtained S-parameters in Figure 17a,b, the final prototype of the designed BLC has good performance at 750 MHz with a bandwidth of 200 MHz, which provides more than 26% FBW. Moreover, it provides wide rejection band from 1.5 GHz to 5.4 GHz, which suppresses the 2nd to 7th harmonics.

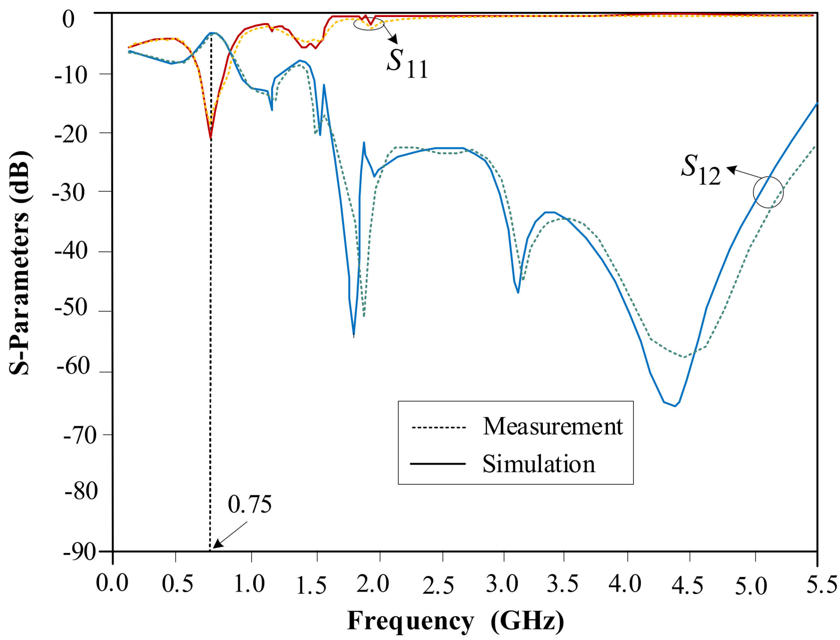

(**a**)

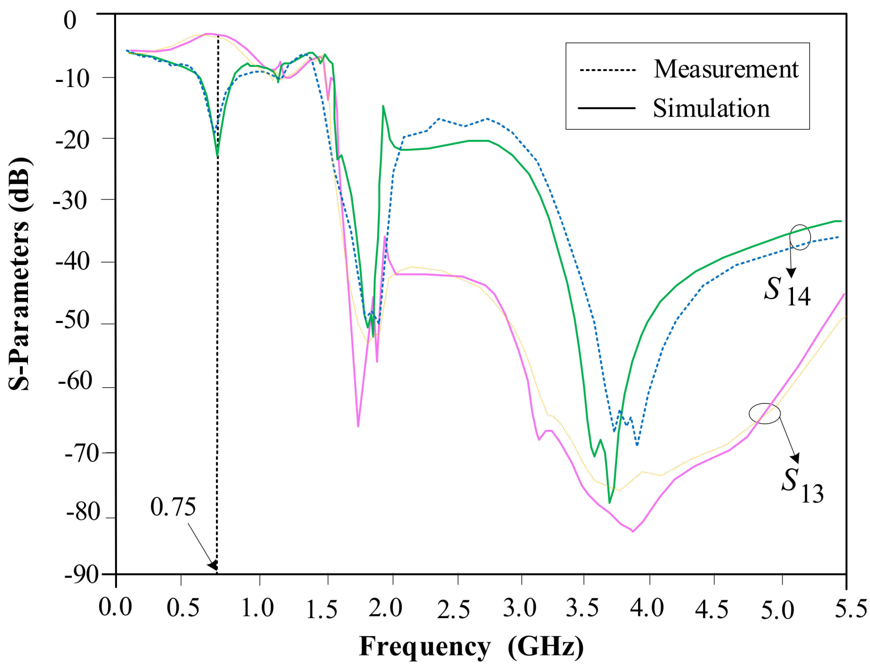

(**b**)

Figure 17. Measurement and EM simulation of the S-parameters with respect to frequency for the final prototype of the designed BLC. (**a**) The values of $|S_{11}|$, and $|S_{12}|$ parameters. (**b**) The values of $|S_{13}|$, and $|S_{14}|$ parameters.

In Figure 18, the measurement and EM simulation results for the output ports phase difference are depicted. As the results show, at 750 MHz, the phase difference is −270.5°, which shows good performance of the final prototype of the designed coupler.

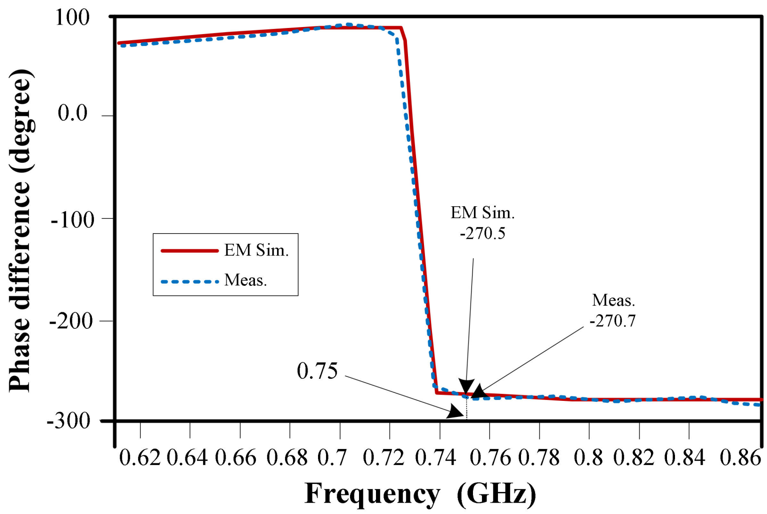

Figure 18. Measurement and EM simulation of the output ports' phase difference.

In Table 3, some related couplers, which were published in recent years, are compared with the final prototype of the designed coupler.

Table 3. Performance comparison between the final prototype of the designed coupler and some related works.

Ref.	Reduction Size (%)	IL (dB)	RL (dB)	Isolation (dB)	Freq. (GHz)	FBW (%)	Size (λ × λ)	Suppressed Harmonics	
								Num.	Details
[36]	66%	1	27	20	0.93	11	0.14λ × 0.15λ	0	-
[37]	62%	1	20	28	1.5	20	0.15λ × 0.16λ	0	-
[38]	-	1.4	-	15	1.87	3.5	0.33λ × 0.42λ	0	-
[39]	73%	-	30	30	1	13.6	0.125λ × 0.135λ	1	2nd: 18 dB
Conv. Coupler	-	0.2	35	35	0.75	20	0.25λ × 0.25λ	0	-
This work	84%	0.3	20	20	0.75	26	0.08λ × 0.12λ	6	2nd: 20 dB 3rd: 23 dB 4th: 28 dB 5th: 39 dB 6th: 52 dB 7th: 23 dB

IL = insertion loss, RL = return loss, Freq. = frequency, FBW = fractional bandwidth, and Conv. = conventional.

6. Conclusions

A compact branch-line coupler (BLC) with improved harmonic suppression ability is designed, analyzed, and fabricated in this manuscript. In the designed coupler, the main drawbacks of the conventional coupler, which are the large size and harmonics presence in the frequency response, are corrected. The triangular shaped and trapezoidal shaped resonators are incorporated into the proposed resonators to form a compact coupler and provide extra transmission zeros. The design coupler has achieved 2nd to 7th harmonics suppression with a wide rejection band and high attenuation. In addition, the obtained overall size of the fabricated coupler is only 0.08 × 0.12 λg^2, which demonstrates an 84% size reduction.

Author Contributions: Conceptualization, S.R. (Sobhan Roshani), S.I.Y. and S.R. (Saeed Roshani); methodology, S.R. (Sobhan Roshani), M.R. and S.R. (Saeed Roshani); software, M.R. and S.R. (Saeed Roshani); validation, S.I.Y.; formal analysis, S.I.Y. and S.R. (Saeed Roshani); investigation, S.R. (Saeed Roshani); resources, S.R. (Sobhan Roshani) and M.R.; writing—original draft preparation, S.I.Y. and S.R. (Saeed Roshani); writing—review and editing, S.R. (Sobhan Roshani) and S.I.Y.; visualization, S.R. (Saeed Roshani) and S.I.Y.; supervision, S.R. (Saeed Roshani); project administration, All authors have read and agreed to the published version of the manuscript.

Funding: This research received no external funding.

Data Availability Statement: All the material conducted in the study is mentioned in article.

Conflicts of Interest: The authors declare no conflict of interest.

References

1. Lalbakhsh, A.; Mohamadpour, G.; Roshani, S.; Ami, M.; Roshani, S.; Sayem, A.S.M.; Alibakhshikenari, M.; Koziel, S. Design of a compact planar transmission line for miniaturized rat-race coupler with harmonics suppression. *IEEE Access* **2021**, *9*, 129207–129217. [CrossRef]
2. Hosseinkhani, F.; Roshani, S. A compact branch-line coupler design using low-pass resonators and meandered lines open stubs. *Turk. J. Electr. Eng. Comput. Sci.* **2018**, *26*, 1164–1170.
3. Lu, K.; Wang, G.-M.; Zhang, C.-X.; Wang, Y.-W. Design of miniaturized branch-line coupler based on novel spiral-based resonators. *J. Electromagn. Waves Appl.* **2011**, *25*, 2244–2253. [CrossRef]
4. Siahkamari, H.; Jahanbakhshi, M.; Al-Anbagi, H.N.; Abdulhameed, A.A.; Pokorny, M.; Linhart, R. Trapezoid-shaped resonators to design compact branch line coupler with harmonic suppression. *AEU-Int. J. Electron. Commun.* **2022**, *144*, 154032. [CrossRef]
5. Kumar, M.; Islam, S.N.; Sen, G.; Parui, S.K.; Das, S. Design of compact Wilkinson power divider and branch line coupler using hairpin based line. *AEU-Int. J. Electron. Commun.* **2019**, *110*, 152825. [CrossRef]
6. Du, R.-N.; Weng, Z.-B.; Zhang, C. A miniaturized filtering 3-dB branch-line hybrid coupler with wide suppression band. *Prog. Electromagn. Res. Lett.* **2018**, *73*, 83–89. [CrossRef]
7. Liao, S.-S.; Peng, J.-T. Compact planar microstrip branch-line couplers using the quasi-lumped elements approach with nonsymmetrical and symmetrical T-shaped structure. *IEEE Trans. Microw. Theory Tech.* **2006**, *54*, 3508–3514. [CrossRef]
8. Jamshidi, M.B.; Roshani, S.; Talla, J.; Roshani, S.; Peroutka, Z. Size reduction and performance improvement of a microstrip Wilkinson power divider using a hybrid design technique. *Sci. Rep.* **2021**, *11*, 7773. [CrossRef]
9. Huang, W.; Liu, C.; Yan, L.; Huang, K. A miniaturized dual-band power divider with harmonic suppression for GSM applications. *J. Electromagn. Waves Appl.* **2010**, *24*, 81–91. [CrossRef]
10. Shum, K.M.; Xue, Q.; Chan, C.H. A novel microstrip ring hybrid incorporating a PBG cell. *IEEE Microw. Wirel. Compon. Lett.* **2001**, *11*, 258–260. [CrossRef]
11. Oraizi, H.; Esfahlan, M. Miniaturization of Wilkinson power dividers by using defected ground structures. *Prog. Electromagn. Res. Lett.* **2008**, *4*, 113–120. [CrossRef]
12. Woo, D.-J.; Lee, T.-K. Suppression of harmonics in Wilkinson power divider using dual-band rejection by asymmetric DGS. *IEEE Trans. Microw. Theory Tech.* **2005**, *53*, 2139–2144.
13. Ghaloua, A.; Zbitou, J.; El Abdellaoui, L.; Latrach, M. Miniaturization and Reduction of Mutual Coupling between Antennas Arrays Using DGS and Planar EBG Structures. In *Emerging Innovations in Microwave and Antenna Engineering*; IGI Global: Hershey, PA, USA, 2019; pp. 192–222.
14. Kumar, K.; Dixit, A.; Kala, P.; Yadav, S.; Pant, R. A Review on Design of Multiband Bandpass Filter Using Different DGS Structures to Enhance the Performance. *J. Circuits Syst. Comput.* **2020**, *29*, 2030012. [CrossRef]
15. Mohamadzade, B.; Lalbakhsh, A.; Simorangkir, R.B.; Rezaee, A.; Hashmi, R.M. Mutual coupling reduction in microstrip array antenna by employing cut side patches and EBG structures. *Prog. Electromagn. Res. M* **2020**, *89*, 179–187. [CrossRef]
16. Lalbakhsh, A.; Afzal, M.U.; Esselle, K.P.; Smith, S.L. Low-cost nonuniform metallic lattice for rectifying aperture near-field of electromagnetic bandgap resonator antennas. *IEEE Trans. Antennas Propag.* **2020**, *68*, 3328–3335. [CrossRef]
17. Parandin, F.; Heidari, F.; Rahimi, Z.; Olyaee, S. Two-Dimensional photonic crystal Biosensors: A review. *Opt. Laser Technol.* **2021**, *144*, 107397. [CrossRef]
18. Parandin, F. Ultra-compact terahertz all-optical logic comparator on GaAs photonic crystal platform. *Opt. Laser Technol.* **2021**, *144*, 107399. [CrossRef]
19. Vahdati, A.; Parandin, F. Antenna patch design using a photonic crystal substrate at a frequency of 1.6 THz. *Wirel. Pers. Commun.* **2019**, *109*, 2213–2219. [CrossRef]

20. Parandin, F.; Kamarian, R.; Jomour, M. Optical 1-bit comparator based on two-dimensional photonic crystals. *Appl. Opt.* **2021**, *60*, 2275–2280. [CrossRef]
21. Karkhanehchi, M.M.; Parandin, F.; Zahedi, A. Design of an all optical half-adder based on 2D photonic crystals. *Photonic Netw. Commun.* **2017**, *33*, 159–165. [CrossRef]
22. Parandin, F.; Moayed, M. Designing and simulation of 3-input majority gate based on two-dimensional photonic crystals. *Optik* **2020**, *216*, 164930. [CrossRef]
23. Parandin, F.; Karkhanehchi, M.M. Low size all optical XOR and NOT logic gates based on two-dimensional photonic crystals. *Majlesi J. Electr. Eng.* **2019**, *13*, 1–5.
24. Parandin, F.; Kamarian, R.; Jomour, M. A novel design of all optical half-subtractor using a square lattice photonic crystals. *Opt. Quantum Electron.* **2021**, *53*, 1–10. [CrossRef]
25. Abdollahi, M.; Parandin, F. A novel structure for realization of an all-optical, one-bit half-adder based on 2D photonic crystals. *J. Comput. Electron.* **2019**, *18*, 1416–1422. [CrossRef]
26. El-Bouslemti, R.; Salah-Belkhodja, F. Miniaturized Power Divider with Planar Stub Structures. *Microw. J.* **2021**, *64*, 54–62.
27. Coromina, J.; Vélez, P.; Bonache, J.; Martín, F. Branch line couplers with small size and harmonic suppression based on non-periodic step impedance shunt stub (SISS) loaded lines. *IEEE Access* **2020**, *8*, 67310–67320. [CrossRef]
28. Singh, R.B.; Weller, T. Miniaturized 20 GHz CPW quadrature coupler using capacitive loading. *Microw. Opt. Technol. Lett.* **2001**, *30*, 3–5. [CrossRef]
29. Eccleston, K.W.; Ong, S.H. Compact planar microstripline branch-line and rat-race couplers. *IEEE Trans. Microw. Theory Tech.* **2003**, *51*, 2119–2125. [CrossRef]
30. Tsai, K.-Y.; Yang, H.-S.; Chen, J.-H.; Chen, Y.-J.E. A miniaturized 3 dB branch-line hybrid coupler with harmonics suppression. *IEEE Microw. Wirel. Compon. Lett.* **2011**, *21*, 537–539. [CrossRef]
31. Coromina, J.; Selga, J.; Velez, P.; Bonache, J.; Martín, F. Size reduction and harmonic suppression in branch line couplers implemented by means of capacitively loaded slow-wave transmission lines. *Microw. Opt. Technol. Lett.* **2017**, *59*, 2822–2830. [CrossRef]
32. Cao, Y.; Wang, Z.; Fang, S.-J.; Liu, Y.A. A miniaturized 3-DB microstrip TRD coupled-line rat-race coupler with harmonics SUPPRESSION. *Prog. Electromagn. Res. C* **2016**, *67*, 107–116. [CrossRef]
33. Kumar, M.; Islam, S.N.; Sen, G.; Das, T.M.; Parui, S.K.; Das, S. Miniaturisation of branch line couplers with a compact transmission line topology based on coupled line section. *IET Microw. Antennas Propag.* **2020**, *14*, 448–455. [CrossRef]
34. Venter, J.J.; Stander, T.; Ferrari, P. *X*-Band Reflection-Type Phase Shifters Using Coupled-Line Couplers on Single-Layer RF PCB. *IEEE Microw. Wirel. Compon. Lett.* **2018**, *28*, 807–809. [CrossRef]
35. Liu, H.; Xun, C.; Fang, S.; Wang, Z.; Liu, D. Coupled-line trans-directional coupler with arbitrary power divisions for equal complex termination impedances. *IET Microw. Antennas Propag.* **2019**, *13*, 92–98. [CrossRef]
36. Wang, Q.; Lim, J.; Jeong, Y. Design of a compact dual-band branch line coupler using composite right/left-handed transmission lines. *Electron. Lett.* **2016**, *52*, 630–631. [CrossRef]
37. Wang, Y.; Ma, K.; Mou, S. A compact branch-line coupler using substrate integrated suspended line technology. *IEEE Microw. Wirel. Compon. Lett.* **2016**, *26*, 95–97. [CrossRef]
38. Shi, J.; Qiang, J.; Xu, K.; Wang, Z.-b.; Lin, L.; Chen, J.-X.; Liu, W.; Zhang, X.Y. A balanced filtering branch-line coupler. *IEEE Microw. Wirel. Compon. Lett.* **2016**, *26*, 119–121. [CrossRef]
39. Honari, M.M.; Mirzavand, R.; Mousavi, P.; Abdipour, A. Class of miniaturised/arbitrary power division ratio couplers with improved design flexibility. *IET Microw. Antennas Propag.* **2015**, *9*, 1066–1073. [CrossRef]
40. Jamshidi, M.B.; Talla, J.; Lalbakhsh, A.; Sharifi-Atashgah, M.S.; Sabet, A.; Peroutka, Z. A Conceptual Deep Learning Framework for COVID-19 Drug Discovery. In Proceedings of the 2021 IEEE 12th Annual Ubiquitous Computing, Electronics & Mobile Communication Conference (UEMCON), New York, NY, USA, 1–4 December 2021; pp. 00030–00034.
41. Jamshidi, M.B.; Roshani, S.; Talla, J.; Lalbakhsh, A.; Peroutka, Z.; Roshani, S.; Sabet, A.; Dehghani, M.; Lotfi, S.; Hadjilooei, F. A Review on Potentials of Artificial Intelligence Approaches to Forecasting COVID-19 Spreading. *Res. Sq.* **2021**, *in preprint*. [CrossRef]
42. Roshani, G.; Nazemi, E.; Roshani, M. Usage of two transmitted detectors with optimized orientation in order to three phase flow metering. *Measurement* **2017**, *100*, 122–130. [CrossRef]
43. Roshani, G.; Nazemi, E. Intelligent densitometry of petroleum products in stratified regime of two phase flows using gamma ray and neural network. *Flow Meas. Instrum.* **2017**, *58*, 6–11. [CrossRef]
44. Roshani, G.; Feghhi, S.; Mahmoudi-Aznaveh, A.; Nazemi, E.; Adineh-Vand, A. Precise volume fraction prediction in oil–water–gas multiphase flows by means of gamma-ray attenuation and artificial neural networks using one detector. *Measurement* **2014**, *51*, 34–41. [CrossRef]
45. Roshani, G.; Nazemi, E.; Feghhi, S. Investigation of using 60Co source and one detector for determining the flow regime and void fraction in gas–liquid two-phase flows. *Flow Meas. Instrum.* **2016**, *50*, 73–79. [CrossRef]
46. Roshani, G.; Nazemi, E.; Feghhi, S.; Setayeshi, S. Flow regime identification and void fraction prediction in two-phase flows based on gamma ray attenuation. *Measurement* **2015**, *62*, 25–32. [CrossRef]
47. Jamshidi, M.B.; Lalbakhsh, A.; Talla, J.; Peroutka, Z.; Roshani, S.; Matousek, V.; Roshani, S.; Mirmozafari, M.; Malek, Z.; Spada, L.L. Deep learning techniques and covid-19 drug discovery: Fundamentals, state-of-the-art and future directions. In *Emerging Technologies During the Era of COVID-19 Pandemic*; Springer: Berlin/Heidelberg, Germany, 2021; pp. 9–31.

48. Jamshidi, M.B.; Lalbakhsh, A.; Alibeigi, N.; Soheyli, M.R.; Oryani, B.; Rabbani, N. Socialization of industrial robots: An innovative solution to improve productivity. In Proceedings of the 2018 IEEE 9th Annual Information Technology, Electronics and Mobile Communication Conference (IEMCON), Vancouver, BC, Canada, 1–3 November 2018; pp. 832–837.
49. Jamshidi, M.B.; Alibeigi, N.; Lalbakhsh, A.; Roshani, S. An ANFIS approach to modeling a small satellite power source of NASA. In Proceedings of the 2019 IEEE 16th International Conference on Networking, Sensing and Control (ICNSC), Banff, AB, Canada, 9–11 May 2019; pp. 459–464.
50. Lalbakhsh, A.; Jamshidi, M.B.; Siahkamari, H.; Ghaderi, A.; Golestanifar, A.; Linhart, R.; Talla, J.; Simorangkir, R.B.; Mandal, K. A compact lowpass filter for satellite communication systems based on transfer function analysis. *AEU-Int. J. Electron. Commun.* **2020**, *124*, 153318. [CrossRef]
51. Roshani, G.; Nazemi, E.; Roshani, M. Identification of flow regime and estimation of volume fraction independent of liquid phase density in gas-liquid two-phase flow. *Prog. Nucl. Energy* **2017**, *98*, 29–37. [CrossRef]
52. Nazemi, E.; Feghhi, S.; Roshani, G.; Peyvandi, R.G.; Setayeshi, S. Precise void fraction measurement in two-phase flows independent of the flow regime using gamma-ray attenuation. *Nucl. Eng. Technol.* **2016**, *48*, 64–71. [CrossRef]
53. Roshani, G.H.; Roshani, S.; Nazemi, E.; Roshani, S. Online measuring density of oil products in annular regime of gas-liquid two phase flows. *Measurement* **2018**, *129*, 296–301. [CrossRef]
54. Roshani, G.; Nazemi, E.; Roshani, M. Intelligent recognition of gas-oil-water three-phase flow regime and determination of volume fraction using radial basis function. *Flow Meas. Instrum.* **2017**, *54*, 39–45. [CrossRef]
55. Roshani, G.; Nazemi, E.; Roshani, M. Flow regime independent volume fraction estimation in three-phase flows using dual-energy broad beam technique and artificial neural network. *Neural Comput. Appl.* **2017**, *28*, 1265–1274. [CrossRef]
56. Nazemi, E.; Roshani, G.; Feghhi, S.; Setayeshi, S.; Zadeh, E.E.; Fatehi, A. Optimization of a method for identifying the flow regime and measuring void fraction in a broad beam gamma-ray attenuation technique. *Int. J. Hydrogen Energy* **2016**, *41*, 7438–7444. [CrossRef]
57. Karami, A.; Roshani, G.H.; Nazemi, E.; Roshani, S. Enhancing the performance of a dual-energy gamma ray based three-phase flow meter with the help of grey wolf optimization algorithm. *Flow Meas. Instrum.* **2018**, *64*, 164–172. [CrossRef]
58. Jamshidi, M.; Lalbakhsh, A.; Talla, J.; Peroutka, Z.; Hadjilooei, F.; Lalbakhsh, P.; Jamshidi, M.; la Spada, L.; Mirmozafari, M.; Dehghani, M. Artificial intelligence and COVID-19: Deep learning approaches for diagnosis and treatment. *IEEE Access* **2020**, *8*, 109581–109595. [CrossRef] [PubMed]
59. Jamshidi, M.; Lalbakhsh, A.; Lotfi, S.; Siahkamari, H.; Mohamadzade, B.; Jalilian, J. A neuro-based approach to designing a Wilkinson power divider. *Int. J. RF Microw. Comput. Aided Eng.* **2020**, *30*, e22091. [CrossRef]
60. Jamshidi, M.B.; Lalbakhsh, A.; Mohamadzade, B.; Siahkamari, H.; Mousavi, S.M.H. A novel neural-based approach for design of microstrip filters. *AEU Int. J. Electron. Commun.* **2019**, *110*, 152847. [CrossRef]
61. Karami, A.; Roshani, G.; Khazaei, A.; Nazemi, E.; Fallahi, M. Investigation of different sources in order to optimize the nuclear metering system of gas–oil–water annular flows. *Neural Comput. Appl.* **2020**, *32*, 3619–3631. [CrossRef]
62. Roshani, G.; Hanus, R.; Khazaei, A.; Zych, M.; Nazemi, E.; Mosorov, V. Density and velocity determination for single-phase flow based on radiotracer technique and neural networks. *Flow Meas. Instrum.* **2018**, *61*, 9–14. [CrossRef]
63. Sattari, M.A.; Roshani, G.H.; Hanus, R.; Nazemi, E. Applicability of time-domain feature extraction methods and artificial intelligence in two-phase flow meters based on gamma-ray absorption technique. *Measurement* **2021**, *168*, 108474. [CrossRef]
64. Roshani, M.; Sattari, M.A.; Ali, P.J.M.; Roshani, G.H.; Nazemi, B.; Corniani, E.; Nazemi, E. Application of GMDH neural network technique to improve measuring precision of a simplified photon attenuation based two-phase flowmeter. *Flow Meas. Instrum.* **2020**, *75*, 101804. [CrossRef]
65. Roshani, M.; Phan, G.; Faraj, R.H.; Phan, N.-H.; Roshani, G.H.; Nazemi, B.; Corniani, E.; Nazemi, E. Proposing a gamma radiation based intelligent system for simultaneous analyzing and detecting type and amount of petroleum by-products. *Nucl. Eng. Technol.* **2021**, *53*, 1277–1283. [CrossRef]
66. Roshani, M.; Phan, G.T.; Ali, P.J.M.; Roshani, G.H.; Hanus, R.; Duong, T.; Corniani, E.; Nazemi, E.; Kalmoun, E.M. Evaluation of flow pattern recognition and void fraction measurement in two phase flow independent of oil pipeline's scale layer thickness. *Alex. Eng. J.* **2021**, *60*, 1955–1966. [CrossRef]
67. Dubovitskiy, M.A.; Pashaev, S.Y.; Zhukov, A.O. Machine Learning Based Computational Electromagnetic Methods for Intelligence CAD/CAE Application. In Proceedings of the 2021 3rd International Youth Conference on Radio Electronics, Electrical and Power Engineering (REEPE), Moscow, Russia, 11–13 March 2021; pp. 1–6.
68. Motaqi, A.; Helaoui, M.; Boulejfen, N.; Chen, W.; Ghannouchi, F. Artificial Intelligence based Power-Temperature Inclusive Digital Pre-Distortion. *IEEE Trans. Ind. Electron.* **2021**, 1. [CrossRef]
69. Pozar, D.M. *Microwave Engineering*; John Wiley & Sons: Hoboken, NJ, USA, 2011; pp. 203–210.
70. Hong, J.-S.G.; Lancaster, M.J. *Microstrip Filters for RF/Microwave Applications*; John Wiley & Sons: Hoboken, NJ, USA, 2004; pp. 84–99.